International Journal of Innovative Research in Engineering & Management (IJIREM)
ISSN: 2350-0557, Volume-5, Issue-1, January-2018
DOI: 10.21276/ijirem.2018.5.1.6

Numerical Simulation of Impact

Édio Pereira Lima Júnior
Mechanical Engineering Department, Military Institute of Engineering - IME, Rio de Janeiro, Brazil

Wendel Rodrigues Miranda
Mechanical Engineering Department, Military Institute of Engineering - IME, Rio de Janeiro, Brazil

André Luiz Tenório Rezende
Mechanical Engineering Department, Military Institute of Engineering - IME, Rio de Janeiro, Brazil

Arnaldo Ferreira
Mechanical Engineering Department, Military Institute of Engineering - IME, Rio de Janeiro, Brazil

ABSTRACT
The dynamic study of colliding objects is an important branch of study in engineering due to recurrence of impacts in real situations such as car crashes, gunshot or bird impacts, for example. The pressure profiles are determined by shock wave propagation phenomena, where the stress tensor determination is necessary for the development of new materials and structures, regarding aspects such as safety. Numerical simulation can be applied to approximate the solution of shock wave problems where materials are submitted to high strain rates. In this paper a methodology to simulate problems involving shock wave propagation is present. To avoid numerical complications associated with highly distorted grid due the large deformation, the numerical meshless method smoothed particle hydrodynamic (SPH) was employed to approximate the derivative governing equations. As the methodology is general this work aims academic objectives, and to be applicable the only changes are in the initial conditions of particles. To evaluate the numerical code a particular case with analytical solution was tested, a one-dimensional plate impact ignoring the deviatory stress showed a percentage error less than 0.1665 % in pressure profiles. Another two-dimensional impact example was presented in this work with the deviatory tensor considered.

Keywords – impact, shock wave propagation, SPH

1. INTRODUCTION
In many situations, the stress state is assumed to be reached instantaneously as consequence of an external force. Many branches of science use this hypothesis to model the phenomenon under observation. This approach is adequate when the observation time is much larger than the time necessary to reach equilibrium [3].

In several situations, the dynamics of the event requires a special treatment where the inertia and internal kinematics of materials become important [10]. The dynamic behavior of materials in impact problems is necessary due the short duration of the collision. Examples of other situations that require dynamic treatment are explosive detonations [6] and metal-explosive interaction [1].

The impact causes the propagation of a pressure pulse in the bodies involved. The shock wave propagation phenomenon is determined by the high strain rates and pressures considerably higher than the yield strength. The material behavior can be classified as elastic, plastic or hydrodynamic [15]. The hydrodynamic classification is usually used for high-velocity impact, where often the deviator stress tensor is neglected and medium can be treated as a non-viscous compressible fluid [2].

The impact and pressure pulse transient propagation is motivated by the recurrence in real life such as car crashes, meteorite or fire gun projectile impacts and soft-body impact on composites like bird impact on airplane glasses. Estimating the dynamic response to intense impulsive loading assists the development of materials for specific.

The Smoothed Particle Hydrodynamics (SPH) is a computational meshless method that can be used to approximate the derivative governing equations for large deformations problems. The SPH was initially applied to astrophysical problems [9, 11] after the method was adapted to simulate shocks waves by introducing artificial viscosity [12] finally it was extended the use for the dynamic response of materials [5]. Many other applications are possible for this numerical method [8].

This paper presents the methodology for simulation of problems considering the dynamic behavior of materials. The governing equations, the Rankine-Hugoniot jump equations and the Mie-Grüneissen equations of state (EOS). The integration of SPH approach of governing equations estimates deformation, particle velocity and pressure pulse. This work is of academic importance due the generality of theory and can be applicable to specific problems by changing the initial conditions of simulation. Because kernel approach in SPH is defined by relative particle positions the simulations in one, two and tree-dimensions can be easily performed.

To present the efficiency of numerical simulation a hydrodynamic one-dimension impact was simulated. This particular case has analytical solution and showed a percentage error less than 0.1665 % in pressure.

In a second step, the pressure contour profiles resulting from a two-dimensional impact are presented, in which a flat projectile

impact a target plate with a circular hole. The results are compared with the case of a target plate without the hole. The constitutive model adopted was the elastic perfectly plastic and the deviatory was considered.

2. METHODOLOGY

This section provides the mathematical development of shock wave propagation in a condensate medium.

2.1 Governing equations

The SPH is a discrete element method based on a Lagrangian coordinate system. This study assumes that the solid subjected to a pressure pulse has a hydrodynamic response with the deviator stress tensor being considered in the equations. The equations 1, 2 and 3 refer to the conservation equations of mass, momentum and energy, respectively [8].

$$\frac{D\rho}{Dt} = -\rho \frac{\partial v^{\alpha}}{\partial x^{\alpha}} \tag{1}$$

$$\frac{Dv^{\alpha}}{Dt} = \frac{1}{\rho} \frac{\partial \sigma^{\alpha\beta}}{\partial x^{\beta}} \tag{2}$$

$$\frac{Du}{Dt} = \frac{\sigma^{\alpha\beta}}{\rho} \frac{\partial v^{\alpha}}{\partial x^{\beta}} \tag{3}$$

where ρ, v, t, σ, x and u represent, respectively, density, velocity vector, time, stress tensor, vector position and internal energy. The symbols α and β denotes the coordinate directions.

2.2 Deviator stress tensor

The stress tensor employed in Equation 2 can be decomposed into hydrostatic stress and deviator stress tensor components. The hydrostatic tensor ($P\delta^{\alpha\beta}$) is associated with the pressure P determined by the EOS and represents the mean normal stress of $\sigma^{\alpha\beta}$ and the deviator stress ($S^{\alpha\beta}$) indicates the deviation of the stress tensor from the hydrostatic axis in Equation 4 below.

$$\sigma^{\alpha\beta} = -P\delta^{\alpha\beta} + S^{\alpha\beta} \tag{4}$$

It is assumed that the generalized Hooke's Law is the constitutive relationship for elastic deformation. The time derivative of deviator stress is related with the strain rate $\dot{\varepsilon}^{\alpha\beta}$ and the rotational rate $\dot{\omega}^{\alpha\beta}$ by the following equation [5]:

$$\dot{S}^{\alpha\beta} = 2G\left(\dot{\varepsilon}^{\alpha\beta} - \dot{\varepsilon}^{\gamma\gamma}/3\right) + S^{\alpha\gamma}\dot{\omega}^{\beta\gamma} + S^{\gamma\beta}\dot{\omega}^{\alpha\gamma} \tag{5}$$

where G is the modulus of elasticity in shear and γ denote a coordinate direction. The strain and the rotational rates are defined as follow:

$$\dot{\varepsilon}^{\alpha\beta} = \left(\partial v^{\alpha}/\partial x^{\beta} + \partial v^{\beta}/\partial x^{\alpha}\right)/2 \tag{6}$$

$$\dot{\omega}^{\alpha\beta} = \left(\partial v^{\alpha}/\partial x^{\beta} - \partial v^{\beta}/\partial x^{\alpha}\right)/2 \tag{7}$$

The Von Mises yield surface based in the maximum distortion energy defines the separation between the elastic and plastic flow for an elastic perfectly plastic constitutive model. We can define a parameter θ that is directly related to the second invariant of the deviator stress tensor:

$$\theta = \left(S^{\alpha\beta}S^{\beta\alpha}\right)^{1/2} \tag{8}$$

The flow is elastic if $\theta \leq \sigma_Y(2/3)^{1/2}$ and plastic otherwise, where σ_Y is the dynamic yield limit. If the integrated deviator stress of Equation 5 is in plastic flow, the deviator stress must be scaled back to the yield surface multiplying the deviator stress obtained by $\sigma_Y(2/3)^{1/2}/\theta$.

2.3 Shock wave propagation

The propagation of shock waves is based on the principles of conservation of mass, momentum and energy. Due the very small thickness of the shock wave front, it is modeled as a discontinuity that separates the undisturbed material from the region under effect of the pressure pulse. With the discontinuity hypothesis and knowing the velocity of the wave front propagation, the quantities before and after the passage of wave can be related. Figure 1 show a scheme of the shock wave discontinuity.

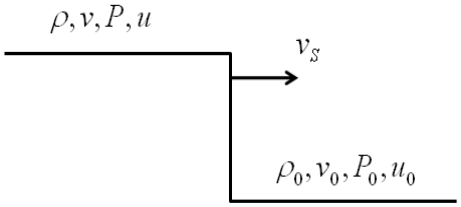

Figure 1. Shock wave discontinuity (adapted from [10]).

The EOS of a material describes empirically the relationship between the shock velocity (v_S) and the particle velocity (v_P) [10]. Experimentally, the linear relationship is a good approximation to relate these velocities for a metallic solid medium [14], where c_0 and s are the interpolation constants.

$$v_S = c_0 + sv_P \tag{9}$$

Considering the initial medium velocity and pressure negligible when compared with the values reached by the shock wave, the algebraic conservation equations and the EOS of a material (Equation 9) yield:

$$P_H = \rho v_s v_p \tag{10}$$

$$u_H = \frac{P_H}{2}\left(V_0 - V\right) \tag{11}$$

where V_0-V is the change in specific volume and the subscript H indicates the values given by the Rankine-Hugoniot jump equations. The pressure and energy calculated with Equations 10 and 11 do not consider thermal effects because time is in the order of nanoseconds. The internal energy is directly obtained from Equation 3 and the difference from the values given by Equation 11 defines how the hydrostatic pressure is away from the value obtained using the Rankine-Hugoniot Equations 10 and 11. The Mie-Grüneissen EOS based on quantum mechanics provides a correction to equation 10 introducing the Mie-Grüneissen constant γ_0 [10]:

$$P = P_H + \frac{\gamma_0}{V_0}\left(u - u_H\right) \tag{12}$$

2.4 Numerical Model – Smoothed Particle Hydrodynamics

The SPH method is a numerical approach of a function *f*, in a point defined by a vector *x*, the integral representation in a domain Ω and associated with a smoothing kernel function *W* [7]. The domain Ω called support domain contains the points under consideration and defines the neighborhood points by vectors *x´*. The characteristic length *h* indicates the length of the computational domain for integration.

$$f(x)=\int_{\Omega} f(x')W(x-x',h)dx' \tag{13}$$

The computational integration takes the form of a summation and the infinitesimal volume is represented by mass and density ratio. The subscripts *i* and *j* designate particles. The kernel function is calculated with the mean characteristic length (h_{ij}) for each pair *i* and *j* and the summation is performed over all the *N* particles in the support domain.

$$f(x_i)=\sum_{j=1}^{N}\frac{m_j}{\rho_j}f(x_j)W_{ij} \tag{14}$$

The spatial derivatives of Equation 14 depend exclusively of the kernel gradient and relative particles positions:

$$\nabla f(x_i)=\sum_{j=1}^{N}\frac{m_j}{\rho_j}f(x_j)\nabla W_{ij} \tag{15}$$

The hypothesis of discontinuity of the wave front introduces numerical instability due the high pressure gradients involved. Thus, a viscosity term is introduced to maintain numerical stability. This term is nonzero only for $v_{ij}.x_{ij} < 0$, where vij and xij are relative vectors $v_{ij} = v_i - v_j$ and $x_{ij} = x_i - x_j$ [12], and assumes the value Π_{ij} given by:

$$\Pi_{ij}=\frac{b\phi_{ij}^2-ac_{ij}\phi_{ij}}{\rho_{ij}} \tag{16}$$

In Equation 16 above, c_{ij} and ρ_{ij} are the mean values of the sound velocity and the density, respectively, a and b are the constants of artificial viscosity and the term is defined in Equation 17 below, where the parameter ζ is introduced to avoid a singularity when $x_{ij} \rightarrow 0$.

$$\phi_{ij}=\frac{h_{ij}\mathbf{v}_{ij}\cdot\mathbf{x}_{ij}}{\left|\mathbf{x}_{ij}\right|^2+(\zeta h_{ij})^2} \tag{17}$$

The quantity defined by equation 16 should be incorporated into the equations as a correction to the pressure values.

2.5 Approach of governing equations

The governing equations of the problem can be written using the SPH formulation and incorporate the artificial viscosity term:

$$\frac{D\rho_i}{Dt}=\sum_{j=1}^{N}m_j v_{ij}^{\alpha}\frac{\partial W_{ij}}{\partial x^{\alpha}} \tag{18}$$

$$\frac{Dv_i^{\alpha}}{Dt}=\sum_{j=1}^{N}m_j\left(\frac{\sigma_i^{\alpha\beta}}{\rho_i^2}+\frac{\sigma_j^{\alpha\beta}}{\rho_j^2}+\Pi_{ij}\right)\frac{\partial W_{ij}}{\partial x_i^{\beta}} \tag{19}$$

$$\frac{Du_i}{Dt}=\frac{1}{2}\sum_{j=1}^{N}m_j\left(\frac{p_i}{\rho_i^2}+\frac{p_j}{\rho_j^2}+\Pi_{ij}\right)v_{ij}^{\beta}\frac{\partial W_{ij}}{\partial x_i^{\beta}}+\frac{1}{\rho_i}S_i^{\alpha\beta}\dot{\varepsilon}_i^{\alpha\beta} \tag{20}$$

2.6 Interpolation kernel

The kernel function W_{ij} [13] is calculated for each pair *i* and *j* considering the distance r_{ij} between these particles normalized by h_{ij}:

$$W(R_{ij})=W(r_{ij}/h_{ij})=C_d\begin{cases}1-3R_{ij}^2/2+3R_{ij}^3/4, \text{if } 0\le R_{ij}\le 1\\ (2-R_{ij})^3/4, \text{if } 1\le R_{ij}<2\\ 0, \text{if } R_{ij}\ge 2\end{cases} \tag{21}$$

where the normalization constant C_d is $2/3h_{ij}$, $10/7\pi h_{ij}^2$ and $1/\pi h_{ij}^3$ for 1, 2 and 3 dimensional space, respectively.

3. RESULTS AND DISCUSSION

This section presents the solution of three impact simulations with plates of Al 2024. The first solution represents a one-dimensional impact which is simulated in order to evaluate the simulations. The second example presents a two-dimensional simulation of plate impact. The last solution presents the same two-dimensional plate impact but the target plate with a hole in its center.

In all the three simulations, the constants *a* and *b* for artificial viscosity were set equal 1 and ζ was assumed to be equal to 0.1; the characteristic length *h* was modeled to follow the change in particle density.

3.1 One-dimensional impact

In order to evaluate the accuracy of the computational code, a 5 mm thickness projectile at 1.0 km/s was simulated impacting a target plate of 50 mm thickness initially at rest, neglecting the deviator stress tensor to compare with analytical solutions. Both plates were of Al 2024 and the shock parameters are given in table 1. The target plate was represented by 4,000 particles and the projectile plate by 400 particles.

Table 1. Shock parameters of Al 2024 [4]

Material	ρ_0 (g/cm³)	c_0 (km/s)	s (km/s)	γ_0
Al 2024	2.785	5.328	1.338	2.0

As both plates were of same material they have the same shock impedance, particle velocities in the region affected by the shock wave must have one half of impact velocity (0.5 km/s). According Equation 9 the shock wave velocity in both plates was 5.9970 km/s. Equation 10 gives the compressive pulse of 8.3508 GPa. At 0.8338 μs the compressive shock wave reaches the free surface of the projectile plate (left part in Figure 2) and reflected as a tensile pulse of 8.3508 GPa, the interact of pulses defines the pressure profile: a plateau of 8.3508 GPa and length of 10 mm, twice the of projectile length.

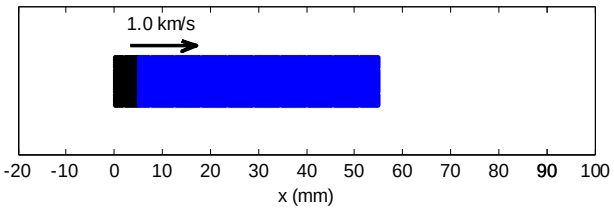

Figure 2. Initial configuration: ■ flying plate, ■ target plate.

.

After the shock reflection, the plateau of wave profile tends to decrease in length because the velocity of the release shock wave is larger than that of the shock front. Figure 3 illustrates the simulated results at 1.0, 5.0 and 8.0 μs, as well as the theoretical position of the wave front.

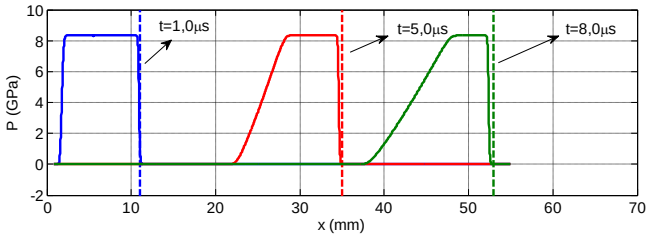

Figure 3. Wave profile at time 1.0, 5.0 and 8.0 μs.

The estimated compressive stresses approach were 8.3389 GPa at 1.0 μs and 8.3369 GPa at 5.0 and 8.0 μs; the percentage errors were -0.1425% and -0.1665%, respectively. The target plate thickness was chosen in function of the time steps presented, if a 100 mm thickness was simulated as in the two-dimensional case, no influence will be noted in Figure 2 because changes will occurs only after the passage of the front.

3.2 Two-dimensional impact

In this second example, a two-dimensional projectile plate with 5.0 mm thickness and 100.0 mm height impacts, at same velocity of one dimensional case 1.0 km/s, to a target square plate with 100.0 mm. Figure 4 shows the initial condition for this case. The shock parameters are given in Table 1. The target plate was represented by 40,000 particles and the flying plate by 2,000 particles

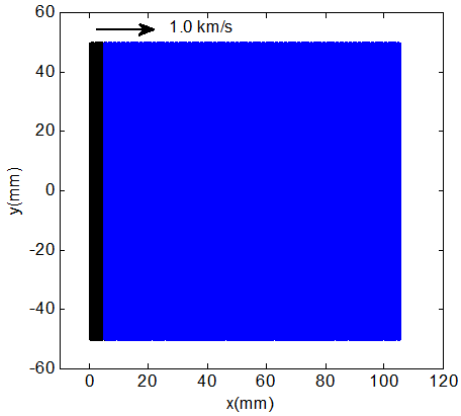

Figure 4. Initial configuration: ■ flying plate, ■ target plate.

The compressive stress pulse originated from the collision moves initially in a plane parallel to the plane of impact. Since the impact is simulated in two dimensions, the material also shows a deformation perpendicular to the impact velocity direction, which decrease density near the horizontal edges and as consequence compressive stress in this. A region with higher pressure is observed along the axis of symmetry (y=0) in Figure 5.

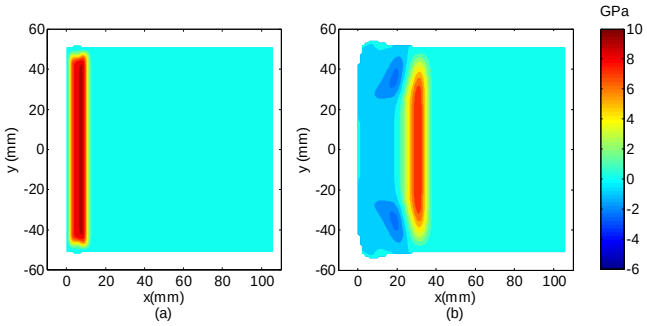

Figure 5. Pressure profile: (a) 1.0 μs and (b) 5.0 μs.

Figure 5 (a) shows the pressure stress profile at 1.0 μs; the maximum compressive stress calculated was 8.5855 GPa, which is 2.8105% larger than the value expected one-dimensional theory. The values observed in the wave front has a numerical oscillation that is smoothed by the viscous term introduced in calculation, in the near the shock front the compressive stress is approximately 8.2051 GPa, which is 1.7447% lower than the analytical solution for one dimension. These compressive stress values indicate that the simulation is in agreement with the one-dimensional analytical solutions 1.0 μs after the impact.

Figure 5 (b) shows the pressure stress profile at 5 μs. The central region of the target plate (y=0) was subjected to higher compression and higher pressure, as shown in Fig. 5. Another important fact is that high pressures stress in the central region lead to vertical acceleration and particles at the periphery of the plate are subjected to a higher vertical velocity, which results in tensile stress zones shown in Figure 5 (b) as consequence of density become less than initial conditions. Therefore, in the two-dimensional deformation study the attenuation of pressure stress occurs sooner than in the one-dimensional study. At 5.0 μs the maximums compressive pressure stress calculated was 7.3769 GPa and tensile stress was 2.4343 GPa.

Figure 6 shows the pressure contours at 10.0 μs and 15.0 μs. In both figures, pressures stresses were smaller than in the one-dimensional solution. Figure 6 (a) shows the profile at 10.0 μs, the maximums pressure stress was 6.0416 GPa and tensile stress was 2.2091 GPa. Figure 6 (b) shows the profile at 15.0 μs, the maximum pressure stress was 4.9634 GPa and the tensile stress in traction was 2.9267 GPa.

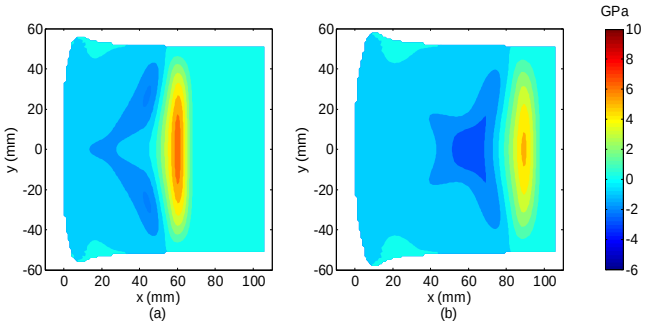

Figure 6. Pressure profile: (a) 10.0 µs and (b) 15.0 µs.

3.3 Two-dimensional impact with a hole in the plate

This third case is a modification of the second removing a circular area with radius 20.0 mm in the center of target as illustrated in Figure 7. The objective was to study the influence of pressure pulse reflection by the hole. Adding a hole, the target plate was represented by 34,976 particles and the projectile particles were unchanged (2,000 particles).

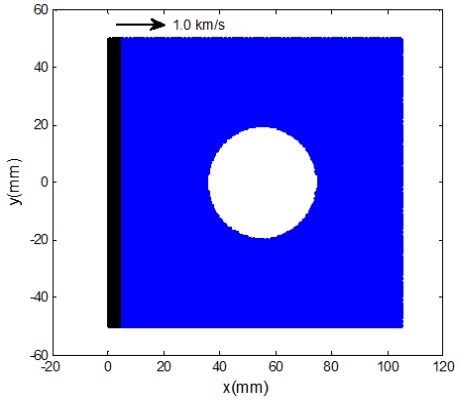

Figure 7. Initial configuration for target plate with hole: ■ flying plate, ■ target plate.

In order to compare the results with the last case, the figures were presented for the same output steps as those of Figures 5 and 6. Figure 8 (a) and (b) present the pressure contours at 1.0 µs and 5.0 µs, respectively, in this two time steps the pressure stress profiles are practically identical to those of Figure 5 due the characteristic of shock wave propagation. At 1.0 µs, the maximum pressure of 8.5855 GPa evinces it, the same values obtained in the case without hole; at 5.0 µs, the maximums compressive stress was 7.3758 GPa and tensile stress was 2.4343 GPa, here a small difference of -0.0149% was observed due imminence of the shock wave reach the hole, which occurs in the time of 5.0025 µs but affects the support domain in integration.

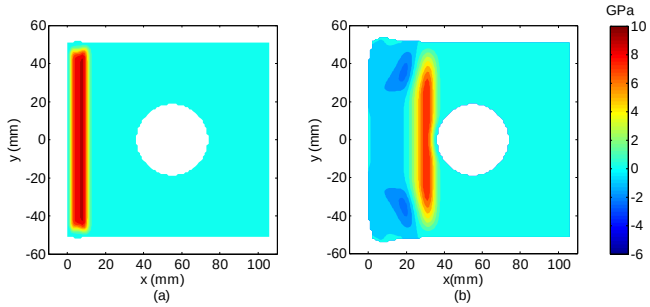

Figure 8. Pressure profile: (a) 1.0 µs and (b) 5.0 µs.

Figure 9 presents the results of pressure pulse reflection in the hole. As shown in Figure 5 and 6, the regions of highest pressure without the hole are along the y=0 axis. In the simulations carried out in this case, the hole in the target plate was in this region. Due to reflection of the shock wave in the hole, the release shock wave interacted with the pressure pulse, increasing the tensile pressure relative to Figure 6 and a compressive pulse is present around the inside hole area (free surface).

Figure 9 (a) shows the pressure profile at 10.0 µs where the maximums compressive stress was 3.1179 GPa and tensile stress was 5.6671 GPa, here the tensile stress reflection was evident and the surface of reflection follow the curvature of the hole. Figure 9 (b) shows the pressure contour at 15.0 µs where the maximums compressive stress was 3.1392 GPa and tensile stress was 3.1455 GPa. These results, when compared with the results obtained in preceding section shows that the compressive stress decreased, while the tensile stress increased, this is an important result due to fact that fracture generally occurs when the material is subjected to tensile loads. An important aspect is that the pressure profile showed were associated with hydrostatic component of stress tensor, while the values were of the order of GPa the plastic deformations and fracture according with Von Mises theory are associated with the deviator stress tensor that assume values considerable less than the hydrostatic tensor component.

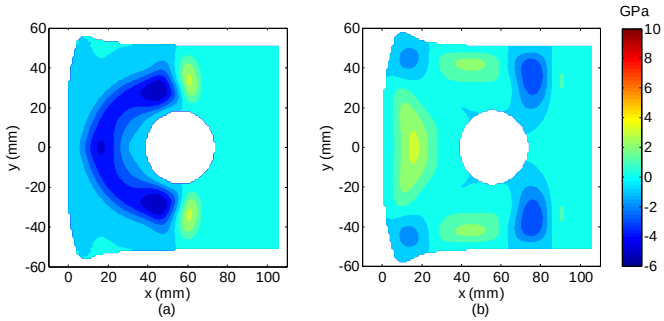

Figure 9. Pressure profile: (a) 10.0 µs and (b) 15.0 µs.

Figure 10 shows the influence of the hole in the pressure pulse profiles. In this plot, the maximums compressive stress and tensile stress are plotted for the time steps displayed. Before the shock wave reaches the hole no significances changes are observed. The shock wave reaches the hole at time of 5.0025 µs and after this time step the two profiles differ because of the shock reflections. An important aspect is that main part of pressure pulse propagation along y=0 axis has to contour a physical discontinuity

in material due the hole, that alter all the simulations after the hole interactions.

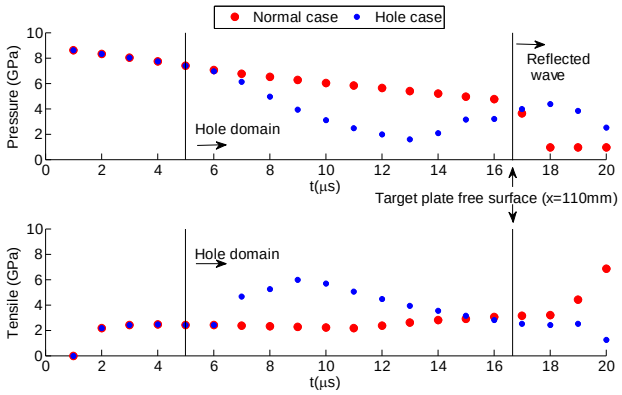

Figure 10. Comparison of compressive and tensile stress in time

4. CONCLUSION

This paper presents a numerical approach to simulate the propagation of a pressure pulse by shock wave propagation with numerical approach using SPH formulation. This procedure is general and can be used to simulate many applicable problems by changing the initial conditions of the simulations, structural analyses can be evaluated for shock wave attenuators to protect important regions of interest for example.

The results of numerical simulation for one-dimensional impact problems were accurate when compared with analytical solutions, percentage error of less than 0.1665% was obtained in the time steps selected. These results are important to show that the code represents adequately the shock propagation phenomena.

The two-dimensional simulations describe the pressure stress along flying and target plates. The pressure profile can be used to estimate the critical stress for fracture in specific problems. It is also possible to obtain information regarding density, velocity, internal energy, effective stress etc.

Another important aspect observed in the simulations is the capability of the code to simulate reflection and interactions of the shock wave. The main features of a change from a compressive stress to a tensile stress were also observed.

REFERENCES

[1] Baêta-Neves, A. P., Ferreira, A. 2015. Shaped charge simulation using SPH in cylindrical coordinates, *Engineering Computations*. 32, 370-386. DOI= https://doi.org/10.1108/EC-09-2013-0221.

[2] Chou, P. C., Hopkins, A. K. 1972. Dynamic response of materials to intense impulsive loading. Air Force Materials Laboratory, Wright-Patterson AFB, OH.

[3] Kolsky, H. 1963. Stress Waves in Solids. Dover Publications, Mineola, NY.

[4] Lee, W. H. 2006. Computer simulation of shaped charge problems. World Scientific Publishing, Hackensack, NJ.

[5] Libersky, L. F., Petschek, A. G., Carney, T. C., Hipp, J. R., Allahdade, F. A. 1993. High strain lagrangian hydrodynamics: a three-dimensional SPH code for dynamic material response", Journal of Comp Physics. 109, 67-75. DOI= 10.1006/jcph.1993.1199.

[6] Lima, E. P. J., Ferreira, A. 2015. Simulação da onda de pressão gerada pela detonação de explosivos utilizando o método SPH. *Revista Militar de Ciência e Tecnologia*, 32. 3-12.

[7] Liu, G. R., Liu, M. B. 2003. Smoothed particle hydrodynamics: a meshfree particle method. World Scientific Publishing, Hackensack, NJ.

[8] Liu, M. B., Liu, G. R. 2010. Smoothed particle hydrodynamics (SPH): an overview and recent developments. Arch Computat Methods Eng. 17, 25-76. DOI= https://doi.org/10.1007/s11831-010-9040-7

[9] Lucy, L. B. 1977. A numerical approach to testing of fission hypothesis. Astronomical Journal. 82, 1013-1024. DOI= http://dx.doi.org/10.1086/112164.

[10] Meyers, M. A. 1994. Dynamic Behavior of Materials. Ed. John Wiley & Son, San Diego, CA. DOI= 10.1002/9780470172278.

[11] Monaghan, J. J., Gingold, R. A. 1977. Smoothed Particle Hydrodynamics: Theory and Applications to Non-Spherical Star. Monthly Notices of the Royal Astronomical Society. 181, 375-389. DOI= https://doi.org/10.1093/mnras/181.3.375

[12] Monaghan, J. J., Gingold, R. A. 1983. Shock Simulation by the particle method SPH. Journal of Comp Physics. 52, 374-383. DOI= https://doi.org/10.1016/0021-9991(83)90036-0

[13] Monaghan, J. J., Lattanzio, J. C. 1985. A refined particle method for astrophysical problems. Astronomy and Astrophysics. 149, 135-143.

[14] Zeldovich, Y. B., Raizer, Y. P. 2002. Physics of Shock Waves and High-Temperature Hydrodynamic Phenomena, Dover Publications, Mineola, NY.

[15] Zukas, J.A., Nicholas, T., Swift, H. F., Greszczuk. L. B., Curran. D. R. 1982. Impact Dynamics. Ed. John Wiley & Son, San Diego, CA.

